Chapter 2
Stiff String Basis Functions

The prediction of natural frequencies of a rotating beam is an important practical problem and is often done using the finite element method [1, 2]. The previous chapter presented the basics of the finite element method as applied to rotating beams. An accurate approach to develop a finite element is to select shape functions which satisfy the static part of the homogenous governing differential equation for the problem [3]. In this chapter, we develop new shape functions using the exact solution of the governing static differential equation of a stiff-string [4]. In order to simplify the analysis required to derive the shape functions, the centrifugal force is assumed as a constant for an element, which leads to the rotating beam equation becoming the stiff-string equation within the element due to the constant applied tension. Fortunately, the stiff-string equation captures the effect of the centrifugal force and also has an analytical solution.

2.1 Stiff String Equation

The partial differential equation for free vibration of a rotating beam was derived in the previous chapter as

$$(EI(x)\, w'')'' + m(x)\, \ddot{w} - (T(x)\, w')' = 0 \tag{2.1}$$

where, $T(x) = \int_x^L m(x)\, \Omega^2\, (R + x)\, dx + F$ is the centrifugal tensile load at a distance x from the axis of rotation, $EI(x)$ is the flexural stiffness, $m(x)$ is the mass per unit length, w is the bending displacement, Ω is the rotation speed, R is the hub radius, L is the beam length and F is the axial force at the end of the beam. Ignoring the inertia

R. Ganguli, *Finite Element Analysis of Rotating Beams*,
Foundations of Engineering Mechanics, DOI 10.1007/978-981-10-1902-9_2

term in Eq. (2.1) yields the static homogeneous equation, which for a uniform beam reduces to,

$$(EI\, w'')'' - (T(x)\, w')' = 0 \tag{2.2}$$

where $T(x) = m\Omega^2(R(L-x) + \frac{L^2-x^2}{2}) + F$. The complicated expression for the $T(x)$ term makes it possible to only obtain series solutions of Eq. (2.2). Most works on rotating beams use cubic shape functions which result from the solution $EIw'''' = 0$ which means that the second term in Eq. (2.2) is completely ignored. Instead, let us consider an approximation which computes the centrifugal stiffening terms in an approximate sense: $T(x) = T = constant$. This approximation effectively reduces the rotating beam Eq. (2.1) to the stiff-string equation given by [4]

$$(EI\, w'')'' + m\ddot{w} - Tw'' = 0 \tag{2.3}$$

The static homogenous form of Eq. (2.3) is

$$(EI\, w'')'' - Tw'' = 0 \tag{2.4}$$

Until this point, no finite element discretization has been introduced. The process of assuming a constant tension as an approximation to the centrifugal stiffening effect may appear to be rather crude. However, if we consider the beam to be divided into N finite elements, T could be assumed to be constant within the element. The constant tension approximation would then become increasingly realistic as the number of elements increase. For an ith element along the beam, the relation between local co-ordinate ($\bar{x}$) and global co-ordinate (x) from Fig. 2.1 is given by $x = x_i + \bar{x}$ where $x_i = \sum_{j=1}^{i-1} l_j$. For a uniform mesh used in this paper, $x_i = (i-1)l$. Using $x = x_i + \bar{x}$ and assuming $EI = EI_i =$ constant for an element, and the tension within the element is a constant(T_i), Eq. (2.4) can be expressed as

$$\frac{d^4w}{d\bar{x}^4} - {C_i}^2 \frac{d^2w}{d\bar{x}^2} = 0 \tag{2.5}$$

where $C_i = \sqrt{\frac{T_i}{EI_i}}$. Equation (2.5), is the governing static homogenous differential equation of a stiff-string in terms of the element co-ordinate for element i. The constant T_i in the expression of C_i for an element is approximated by taking the maximum centrifugal tension which an element experiences. The maximum centrifugal tension T_i for an ith element can be expressed as

$$T_i = \int_{x_i}^{L} m_i(x)\Omega^2(R+x)dx + F = \sum_{j=i}^{j=N} \int_{x_j}^{x_{j+1}} m_j(x)\Omega^2(R+x)dx + F \tag{2.6}$$

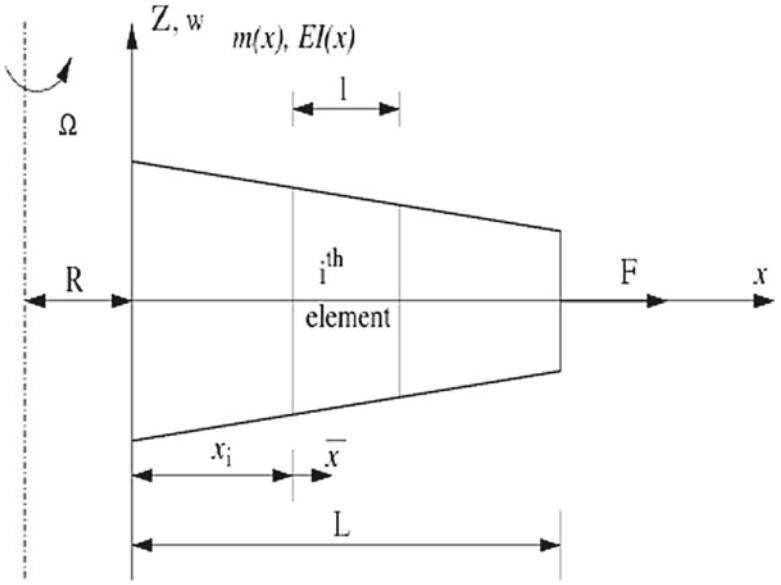

Fig. 2.1 Rotating tapered beam element geometry

Here x_i is the location of the left edge of the element i and $x_{N+1} = L$. The solution of Eq. (2.5) is used as the displacement field.

$$w(x) = a_0 + a_1\bar{x} + a_2 e^{-C_i\bar{x}} + a_3 e^{C_i\bar{x}} \tag{2.7}$$

2.2 Stiff String Basis Functions

Consider the two noded, 4 degree of freedom beam finite element shown in Fig. 2.2. The boundary conditions for the element of length l are given by $w(0) = w_1$, $\frac{dw(0)}{d\bar{x}} = \theta_1 = w_2$, $w(l) = w_3$, $\frac{dw(l)}{d\bar{x}} = \theta_2 = w_4$. Putting Eq. (2.7) into the element boundary conditions yields: $w_1 = a_0 + a_2 + a_3$, $w_2 = a_1 - Ca_2 + Ca_3$, $w_3 = a_0 + a_1 l + a_2 e^{-Cl} + a_3 e^{Cl}$ and $w_4 = a_1 - a_2 Ce^{-Cl} + a_3 Ce^{Cl}$. Here we have dropped the subscript i in C as the entire discussion here is relevant within the element. Solving for a_0, a_1, a_2 and a_3 in terms of the nodal displacements and slopes using the above expressions, w can be approximated by

$$w = w_1 N_1 + w_2 N_2 + w_3 N_3 + w_4 N_4 \tag{2.8}$$

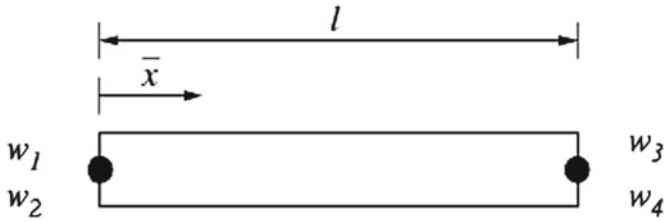

Fig. 2.2 Beam element

where N_1, N_2, N_3 and N_4 are the shape functions and are given as

$$N_1 = \frac{R_1(\bar{x})}{D}, N_2 = \frac{R_2(\bar{x})}{CD}, N_3 = \frac{R_3(\bar{x})}{D}, N_4 = \frac{R_4(\bar{x})}{CD} \tag{2.9}$$

where

$$D = -4 + 2\,e^{Cl} + 2\,e^{-Cl} + Ce^{-Cl}l - Cle^{Cl} \tag{2.10}$$

$$\begin{aligned} R_1(\bar{x}) = &-(-e^{Cl} - e^{-Cl} - Ce^{-Cl}l + 2 + Cle^{Cl} + C\bar{x}e^{-Cl} - C\bar{x}e^{Cl} \\ &-e^{-C\bar{x}+Cl} + e^{-C\bar{x}} + e^{C\bar{x}} - e^{C\bar{x}-Cl}) \end{aligned} \tag{2.11}$$

$$\begin{aligned} R_2(\bar{x}) = &\, e^{Cl} - Cle^{Cl} - e^{-Cl} - Ce^{-Cl}l + C\bar{x}e^{Cl} + C\bar{x}e^{-Cl} - 2\,C\bar{x} \\ &- e^{-C\bar{x}+Cl} + e^{-C\bar{x}+Cl}Cl + e^{-C\bar{x}} + e^{C\bar{x}-Cl} \\ &+ e^{C\bar{x}-Cl}Cl - e^{C\bar{x}} \end{aligned} \tag{2.12}$$

$$\begin{aligned} R_3(\bar{x}) = &\, (e^{Cl} + e^{-Cl} - 2 + C\bar{x}e^{-Cl} - C\bar{x}e^{Cl} - e^{-C\bar{x}+Cl} + e^{-C\bar{x}} \\ &+ e^{C\bar{x}} - e^{C\bar{x}-Cl}) \end{aligned} \tag{2.13}$$

$$\begin{aligned} R_4(\bar{x}) = &\, (2\,Cl - e^{Cl} + e^{-Cl} - 2\,C\bar{x} + C\bar{x}e^{Cl} + C\bar{x}e^{-Cl} - e^{-C\bar{x}}Cl \\ &- e^{-C\bar{x}} + e^{-C\bar{x}+Cl} + e^{C\bar{x}} - e^{C\bar{x}}Cl - e^{C\bar{x}-Cl}) \end{aligned} \tag{2.14}$$

We call these the stiff string basis functions. For vibration analysis of a stiff string, these basis functions satisfy the static homogenous part of the governing differential equation and therefore yield all the favorable properties discussed in [3]. For a rotating beam, their use is an approximation which will be justified by numerical studies later in this chapter. Note that the stiff string basis functions are now also a function of the non-dimensional rotational speed, element mass and stiffness, mass of outboard elements, beam length and location of the element due to their dependence on $C = \sqrt{\frac{T_i}{EI_i}}$. These shape functions therefore capture the effect of the rotation speed

on the element displacements as well as the fact that different locations contribute differently to the centrifugal stiffening effect.

The analytical limits of the stiff string basis functions as the rotation speed tends to zero is shown in Eqs. (2.15) and (2.16) to become the Hermite cubics.

$$\lim_{C\to 0} N_1 = \frac{2x^3 - 3x^2 l + l^3}{l^3},\ \lim_{C\to 0} N_2 = \frac{x^3 - 2x^2 l + x l^2}{l^2} \tag{2.15}$$

$$\lim_{C\to 0} N_3 = \frac{-2x^3 + 3x^2 l}{l^3},\ \lim_{C\to 0} N_4 = \frac{-x^2 l + x^3}{l^2} \tag{2.16}$$

As the rotation speed tends to infinity, the basis functions N_1 and N_3 become linear and N_2 and N_4 approach zero, as given in Eq. (2.1).

$$\lim_{C\to\infty} N_1 = 1 - \frac{\bar{x}}{l},\ \lim_{C\to\infty} N_2 = 0,\ \lim_{C\to\infty} N_3 = \frac{\bar{x}}{l},\ \lim_{C\to\infty} N_4 = 0 \tag{2.17}$$

Variation of the shape functions along the elements ($N = 1$) is shown in Figs. 2.3 and 2.4 with the conventional Hermite cubic and the stiff string basis functions at a

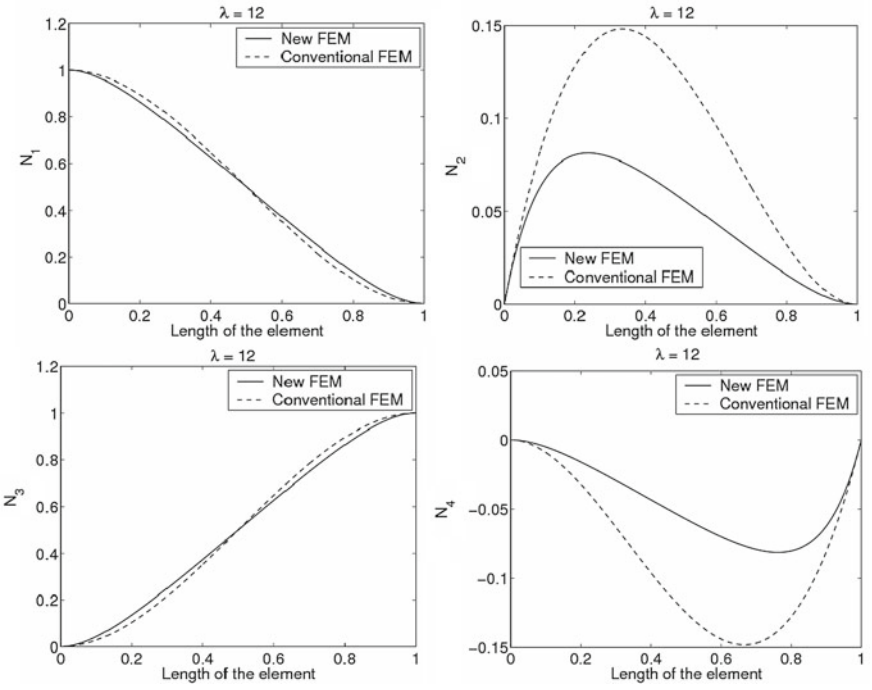

Fig. 2.3 Variation of shape functions along the elements ($N = 1$, $\lambda = 12$) with the new and conventional finite element at high rotation speed

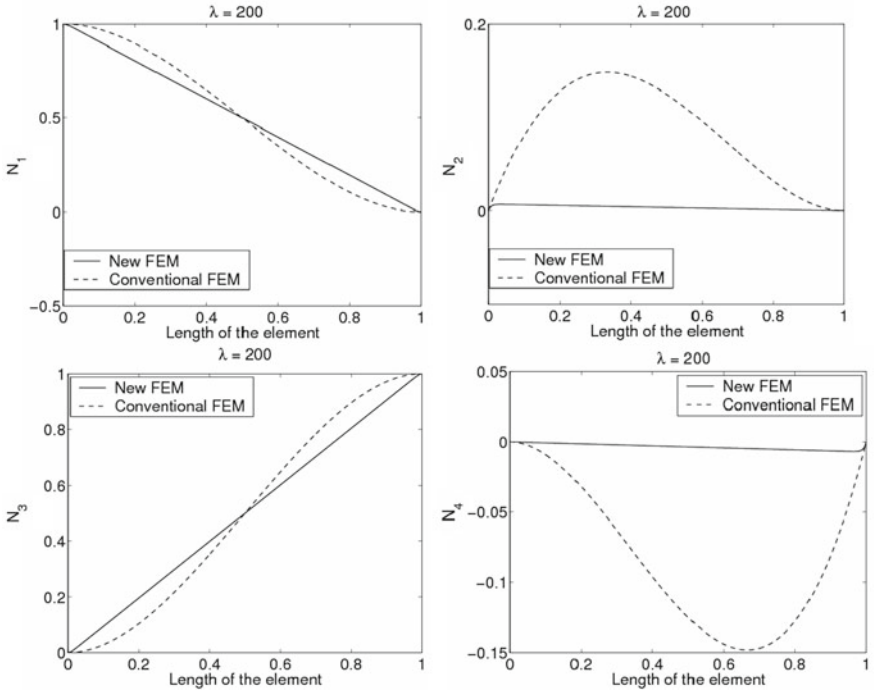

Fig. 2.4 Variation of shape functions along the elements ($N = 1$, $\lambda = 200$) with the new and conventional finite element at very high rotation speed

high ($\lambda = 12$) and very high ($\lambda = 200$) rotation speed, respectively ($\lambda^2 = \frac{m\omega^2 L^4}{EI}$). The difference between the two shape functions is clear. These shape functions therefore capture the effect of the rotation speed on the element displacements. As the rotation speed rises, the stiff string basis functions become almost linear and the rotating beam approaches a rotating string, as is clear from Eq. (2.17). One can also observe from Eq. (2.7) that when $T_i = 0$, w can be represented as a cubic polynomial and when $T_i \to \infty$, the second term dominates and w is a linear function.

The stiff string basis functions are used to develop the finite element equations for free vibration of the rotating beam and numerical results are obtained for a uniform beam and a tapered beam, in the next two sections.

2.3 Uniform Rotating Beam

Tables 2.1 and 2.2 show a comparison of non-dimensional natural frequencies of a rotating uniform cantilever and hinged beam, respectively, with results from [1, 5, 6]. Convergence for the first five modes was achieved using 75 uniform finite elements and the results compare well.

Table 2.1 Comparison of non-dimensional natural frequencies of cantilever uniform beam

Mode	Present-FEM	Wang and Wereley [6]	Wright et al. [5]	Hodges et al. [1]
$\lambda = 12$				
1	13.1702	13.1702	13.1702	13.1702
2	37.6031	37.6031	37.6031	37.6031
3	79.6145	79.6145	79.6145	79.6145
4	140.534	140.534	140.534	N/A
5	220.537	220.536	220.536	N/A

Table 2.2 Comparison of non-dimensional natural frequencies of hinged uniform beam

Mode	Present-FEM	Wang and Wereley [6]	Wright et al. [5]
$\lambda = 12$			
1	12.0000	12.0000	12.0000
2	33.7603	33.7603	33.7603
3	70.8373	70.8373	70.8373
4	126.431	126.431	126.431
5	201.123	201.122	201.122

The new element is now compared with the conventional element with cubic basis functions discussed in Chap. 1. A convergence study is done at two different rotation speeds ($\lambda = 12, \lambda = 200$) on the first three modes, since they are critical for dynamic modeling and modes higher than three show little effect of rotation [2]. For $\lambda = 12$ results in Fig. 2.5, the convergence of the first mode is extremely good, though the second and third mode show slower convergence. For $\lambda = 200$ results in Fig. 2.6, convergence of the second mode also shows an improvement.

2.4 Tapered Rotating Beam

Consider the tapered beam used in [1] with $m(\xi) = m_0\,(1 - 0.5\,\xi)$, and $EI(\xi) = EI_0\,(1 - 0.5\,\xi)^3$. Here m_0 and EI_0 correspond to the value of mass per unit length and flexural rigidity at the thick end of the beam ($\xi = 0$), respectively. Table 2.3 shows the present results and those in [1, 6]. The comparison is very good.

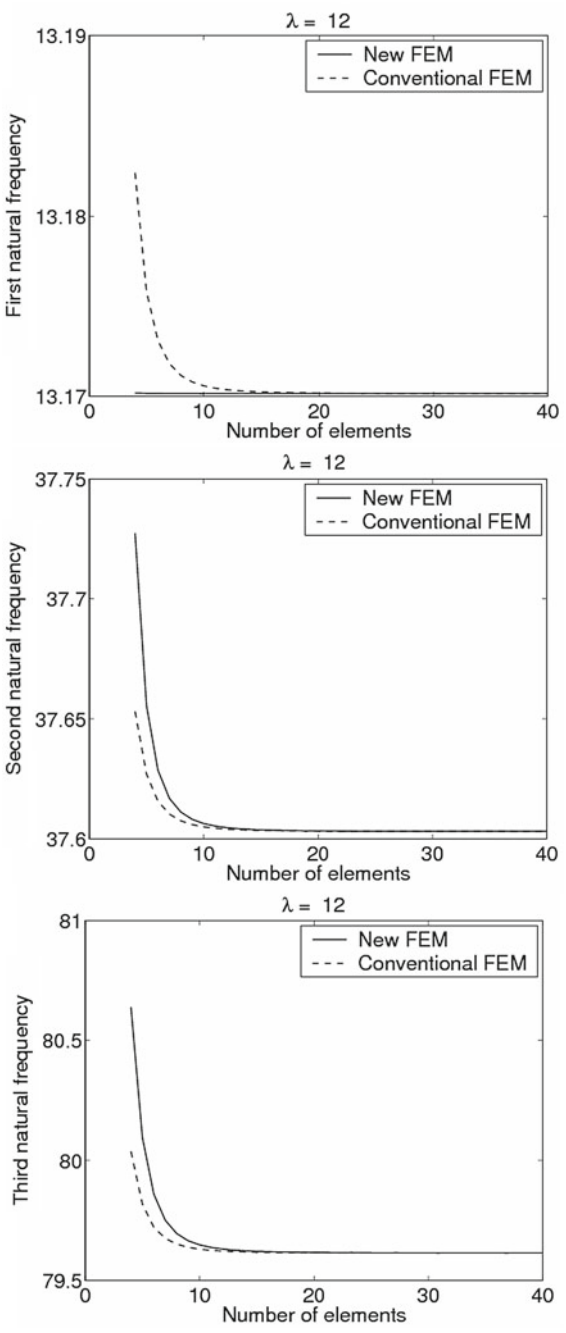

Fig. 2.5 Convergence of the natural frequencies with $\lambda = 12$

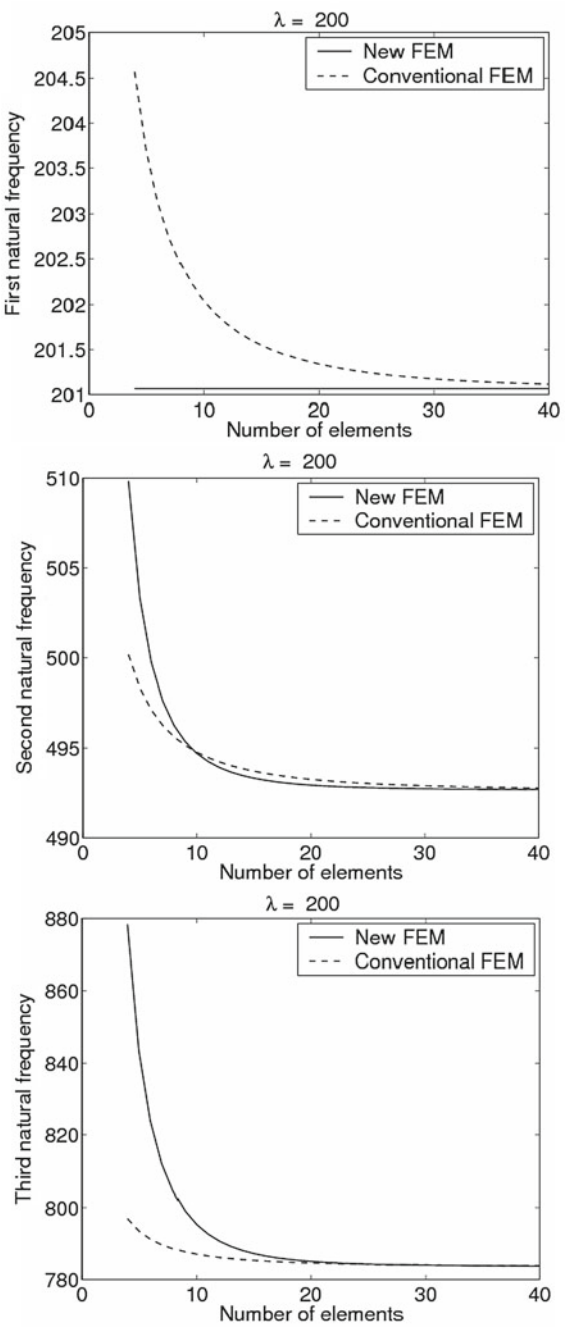

Fig. 2.6 Convergence of the natural frequencies with $\lambda = 200$

Table 2.3 Comparison of non-dimensional natural frequencies of tapered cantilever beam under different rotation speeds

λ	First mode			Second mode			Third mode		
	Present	Ref. [6]	Ref. [1]	Present	Ref. [6]	Ref. [1]	Present	Ref. [6]	Ref. [1]
1	3.9866	3.9866	3.9866	18.4740	18.4740	18.4740	47.4173	47.4173	47.4173
2	4.4368	4.4368	4.4368	18.9366	18.9366	18.9366	47.8717	47.8716	47.8716
3	5.0927	5.0927	5.0927	19.6839	19.6839	19.6839	48.6191	48.6190	48.6190
4	5.8788	5.8788	5.8788	20.6852	20.6852	20.6852	49.6457	49.6456	49.6456
5	6.7434	6.7434	6.7345	21.9053	21.9053	21.9053	50.9339	50.9338	50.9338
6	7.6551	7.6551	7.6551	23.3093	23.3093	23.3093	52.4633	52.4633	52.4633
7	8.5956	8.5956	8.5956	24.8647	24.8647	24.8647	54.2125	54.2124	54.2124
8	9.5540	9.5540	9.5540	26.5437	26.5437	26.5437	56.1596	56.1595	56.1595
9	10.5239	10.5239	10.5239	28.3227	28.3227	28.3227	58.2834	58.2833	58.2833
10	11.5015	11.5015	11.5015	30.1827	30.1827	30.1827	60.5640	60.5639	60.5639
11	12.4845	12.4845	12.4845	32.1085	32.1085	32.1085	62.9830	62.9829	62.9829
12	13.4711	13.4711	13.4711	34.0877	34.0877	34.0877	65.5238	65.5237	65.5237

2.5 Hybrid Basis Functions

Using the stiff string basis function improves FEM performance at the first mode but does not improve performance for higher modes. It is possible to get better results by combining the stiff string basis function with the cubic function. The function assumed for the hybrid basis FE formulation is a linear combination of terms is given as

$$w(\bar{x}) = a_0 + a_1\bar{x} + a_2\bar{x}^2 + a_3\bar{x}^3 + a_4e^{-C_i\bar{x}} + a_5e^{C_i\bar{x}} \tag{2.18}$$

Differentiating Eq. (2.18) with respect to $\bar{x}$ and is given by

$$\frac{dw}{d\bar{x}} = a_1 + 2a_2\bar{x} + 3a_3\bar{x}^2 - a_4C_ie^{-C_i\bar{x}} + a_5C_ie^{C_i\bar{x}} \tag{2.19}$$

It is clearly evident from Eqs. (2.18) and (2.19) that the present basis function is capable of representing a rigid body mode [8] in translation and rotation when only a_0 and a_1 are non-zero respectively. In the present problem the generalized strain and stresses can be attributed to curvature and bending moment and the present interpolation function is capable of representing a constant strain [8] state i.e., capable of representing a constant curvature when only a_2 is non-zero. Hence, Eq. (2.18) represents a complete interpolation function [8].

Consider the three noded, 6 degree of freedom finite element shown in Fig. 2.7. The boundary conditions for the element of length l are given by $w(0) = w_1$, $\frac{dw(0)}{d\bar{x}} = \theta_1 = w_2$, $w(l/2) = w_3$, $\frac{dw(l/2)}{d\bar{x}} = \theta_2 = w_4$, $w(l) = w_5$, $\frac{dw(l)}{d\bar{x}} = \theta_3 = w_6$ Putting Eq. (2.18)

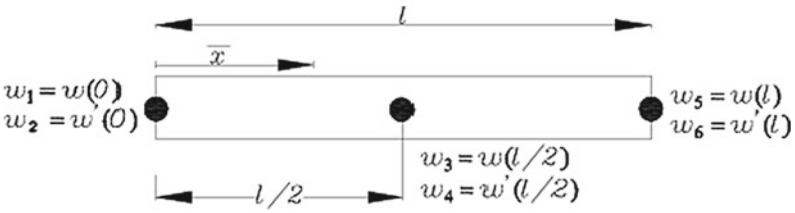

Fig. 2.7 Beam element

into the element boundary conditions yields the following six equations. For further study we have dropped the subscript i in C as the entire discussion here is relevant within the element.

$$w_1 = a_0 + a_4 + a_5 \tag{2.20}$$

$$w_2 = a_1 - Ca_4 + Ca_5 \tag{2.21}$$

$$w_3 = a_0 + a_1(l/2) + a_2(l/2)^2 + a_3(l/2)^3 + a_4e^{-C(l/2)} + a_5e^{C(l/2)} \tag{2.22}$$

$$w_4 = a_1 + 2a_2(l/2) + 3a_3(l/2)^2 - a_4Ce^{-Cl/2} + a_5Ce^{Cl/2} \tag{2.23}$$

$$w_5 = a_0 + a_1l + a_2l^2 + a_3l^3 + a_4e^{-Cl} + a_5e^{Cl} \tag{2.24}$$

$$w_6 = a_1 + 2a_2l + 3a_3l^2 - a_4Ce^{-Cl} + a_5Ce^{Cl} \tag{2.25}$$

Solving for a_0, a_1, a_2, a_3, a_4 and a_5 in terms of the degrees of freedom considered using Eqs. (2.20)–(2.25), w can be approximated by

$$w = w_1 N_1 + w_2 N_2 + w_3 N_3 + w_4 N_4 + w_5 N_5 + w_6 N_6 \tag{2.26}$$

where $N_1, N_2, N_3, N_4, N_5, N_6$ are the interpolating functions derived using the present hybrid basis functions, and are given below.

$$N_1 = \frac{\bar{R}_1(\bar{x})}{-l^2\,D(\bar{x})}, N_2 = \frac{\bar{R}_2\,(\bar{x})}{-l^2 D(\bar{x})}, N_3 = \frac{\bar{R}_3\,(\bar{x})}{l\,D(\bar{x})}, N_4 = \frac{\bar{R}_4\,(\bar{x})}{l^2 D(\bar{x})},$$

$$N_5 = \frac{\bar{R}_5\,(\bar{x})}{-l^2 D(\bar{x})}, N_6 = \frac{\bar{R}_6\,(\bar{x})}{l^2 D(\bar{x})}$$

where

$$\begin{aligned}\bar{R}_1(\bar{x}) = {} & 24\,C\bar{x}l^2e^{Cl} - 5\,e^{C(-\bar{x}+l)}l^3C + 5\,C^2\bar{x}l^3e^{-Cl} + e^{C\bar{x}}l^3C - 64\,C\bar{x}^3e^{1/2\,Cl} \\ & - 64\,C\bar{x}^3e^{-1/2\,Cl} + e^{-C\bar{x}}l^3C - 5\,C^2\bar{x}l^3e^{Cl} + 24\,e^{-1/2\,C(-2\,\bar{x}+l)}l^2 \\ & + 24\,e^{C(-\bar{x}+l)}l^2 + 8\,C^2\bar{x}l^3e^{-1/2\,Cl} - 24\,C\bar{x}l^2e^{1/2\,Cl} - 24\,C\bar{x}l^2e^{-1/2\,Cl} \\ & + 4\,C^2\bar{x}^2l^2e^{-1/2\,Cl} - 4\,C^2\bar{x}^2l^2e^{1/2\,Cl} + 96\,C\bar{x}^2le^{1/2\,Cl} + 96\,C\bar{x}^2le^{-1/2\,Cl} \\ & - 8\,C^2\bar{x}^3le^{-1/2\,Cl} + 4\,l^4C^2e^{1/2\,Cl} + l^4C^2e^{Cl} - l^4C^2e^{-Cl} - 4\,l^4C^2e^{-1/2\,Cl} \\ & + 34\,l^3C - 5\,e^{-C(-\bar{x}+l)}l^3C - 5\,l^3Ce^{-Cl} - 5\,l^3Ce^{Cl} - 8\,e^{1/2\,C(-2\,\bar{x}+l)}l^3C \\ & - 8\,C^2\bar{x}^2l^2e^{-Cl} + 8\,C^2\bar{x}^2l^2e^{Cl} - 36\,C\bar{x}^2le^{Cl} - 4\,C^2\bar{x}^3le^{Cl} - 120\,C\bar{x}^2l \\ & + 96\,C\bar{x}^3 - 8\,e^{-1/2\,C(-2\,\bar{x}+l)}l^3C - 24\,l^2e^{1/2\,Cl} + 24\,l^2e^{-1/2\,Cl} - 8\,C^2\bar{x}l^3e^{1/2\,Cl} \\ & + 8\,C^2\bar{x}^3le^{1/2\,Cl} - 24\,e^{1/2\,C(-2\,\bar{x}+l)}l^2 - 36\,C\bar{x}^2le^{-Cl} - 24\,e^{-C(-\bar{x}+l)}l^2 \\ & + 16\,C\bar{x}^3e^{-Cl} + 16\,C\bar{x}^3e^{Cl} + 4\,C^2\bar{x}^3le^{-Cl} \\ & + 24\,C\bar{x}l^2e^{-Cl} \end{aligned} \tag{2.27}$$

$$\begin{aligned}\bar{R}_2(\bar{x}) = {} & -l^4e^{-C(-\bar{x}+l)}C + 24\,\bar{x}l^2e^{Cl} + 40\,\bar{x}^3Cl + l^4Ce^{-Cl} + 72\,\bar{x}^2le^{1/2\,Cl} \\ & + 32\,\bar{x}^3e^{-1/2\,Cl} + l^4Ce^{Cl} - 24\,\bar{x}l^2e^{-Cl} - l^4e^{C(-\bar{x}+l)}C - 5\,l^3e^{-C(-\bar{x}+l)} \\ & - 2\,l^4e^{1/2\,C(-2\,\bar{x}+l)}C + 5\,l^3e^{C(-\bar{x}+l)} - 4\,\bar{x}^3lCe^{Cl} - 4\,l^3e^{1/2\,C(-2\,\bar{x}+l)} \\ & + 4\,l^3e^{-1/2\,C(-2\,\bar{x}+l)} - 2\,l^4e^{-1/2\,C(-2\,\bar{x}+l)}C + 5\,l^3e^{-Cl} + 34\,\bar{x}l^3C \\ & - 72\,\bar{x}^2l^2C - 12\,\bar{x}l^3Ce^{-1/2\,Cl} - 2\,\bar{x}l^4C^2e^{-1/2\,Cl} - 12\,\bar{x}l^3Ce^{1/2\,Cl} \\ & + 2\,\bar{x}l^4C^2e^{1/2\,Cl} + 28\,\bar{x}^2l^2Ce^{-1/2\,Cl} + 6\,\bar{x}^2l^3C^2e^{-1/2\,Cl} + 28\,\bar{x}^2l^2Ce^{1/2\,Cl} \\ & - 6\,\bar{x}^2l^3C^2e^{1/2\,Cl} - 16\,\bar{x}^3lCe^{-1/2\,Cl} - 4\,\bar{x}^3C^2l^2e^{-1/2\,Cl} - 16\,\bar{x}^3lCe^{1/2\,Cl} \\ & + 4\,\bar{x}^3l^2C^2e^{1/2\,Cl} - 48\,\bar{x}l^2e^{1/2\,Cl} + 2\,l^4Ce^{1/2\,Cl} + 2\,l^4Ce^{-1/2\,Cl} + 48\,\bar{x}l^2e^{-1/2\,Cl} \\ & - 72\,\bar{x}^2le^{-1/2\,Cl} + l^3e^{C\bar{x}} - l^3e^{-C\bar{x}} + 4\,l^3e^{1/2\,Cl} - 4\,l^3e^{-1/2\,Cl} - 32\,\bar{x}^3e^{1/2\,Cl} \\ & - 5\,\bar{x}l^3Ce^{Cl} - 5\,\bar{x}l^3Ce^{-Cl} + 8\,\bar{x}^2l^2Ce^{Cl} + 8\,\bar{x}^2l^2Ce^{-Cl} - 16\,\bar{x}^3e^{-Cl} - 5\,l^3e^{Cl} \\ & - 4\,\bar{x}^3lCe^{-Cl} - 36\,\bar{x}^2le^{Cl} + 36\,\bar{x}^2le^{-Cl} + 16\,\bar{x}^3e^{Cl} \end{aligned} \tag{2.28}$$

$$\begin{aligned}\bar{R}_3(\bar{x}) = {} & -24\,C\bar{x}^2e^{Cl} - 4\,e^{C(-\bar{x}+l)}l^2C - 4\,C^2\bar{x}l^2e^{Cl} - 16\,C^2\bar{x}l^2e^{1/2\,Cl} + 16\,C^2\bar{x}l^2e^{-1/2\,Cl} \\ & + 16\,C^2\bar{x}^2le^{1/2\,Cl} - 16\,C^2\bar{x}^2le^{-1/2\,Cl} + 24\,e^{C(-\bar{x}+l)}l - 24\,e^{-C\bar{x}}l + 24\,e^{C\bar{x}}l \\ & - 24\,e^{-C(-\bar{x}+l)}l - 24\,e^{Cl}l + 24\,e^{-Cl}l + 4\,l^2Ce^{-Cl} + 4\,l^2Ce^{Cl} + 16\,l^2Ce^{1/2\,Cl} \\ & + 16\,l^2Ce^{-1/2\,Cl} + 8\,Cl^2 - 24\,C\bar{x}^2e^{-Cl} - 48\,C\bar{x}l \\ & + 24\,C\bar{x}le^{-Cl} + 4\,C^2\bar{x}l^2e^{-Cl} + 4\,C^2\bar{x}^2le^{Cl} - 4\,C^2\bar{x}^2le^{-Cl} + 24\,C\bar{x}le^{Cl} \\ & - 16\,e^{1/2\,C(-2\,\bar{x}+l)}l^2C - 4\,e^{-C\bar{x}}l^2C - 4\,e^{C\bar{x}}l^2C + 48\,C\bar{x}^2 - 16\,e^{-1/2\,C(-2\,\bar{x}+l)}l^2C \\ & - 4\,e^{-C(-\bar{x}+l)}l^2C \end{aligned} \tag{2.29}$$

$$\begin{aligned}\bar{R}_4(\bar{x}) = {} & 2\,l^4 e^{-C(-\bar{x}+l)}C - 16\,\bar{x}^3 Cl - 2\,l^4 Ce^{-Cl} + 96\,\bar{x}^2 le^{1/2\,Cl} + 64\,\bar{x}^3 e^{-1/2\,Cl} \\ & - 2\,l^4 Ce^{Cl} + 2\,l^4 e^{C(-\bar{x}+l)}C + 8\,l^3 e^{-C(-\bar{x}+l)} - 8\,l^3 e^{C(-\bar{x}+l)} - 24\,\bar{x}^3 lCe^{Cl} \\ & + 16\,l^3 e^{1/2\,C(-2\,\bar{x}+l)} - 16\,l^3 e^{-1/2\,C(-2\,\bar{x}+l)} + 2\,\bar{x}l^4 C^2 e^{Cl} - 2\,l^4 e^{-C\bar{x}}C \\ & - 2\,l^4 e^{C\bar{x}}C - 8\,l^3 e^{-Cl} + 6\,\bar{x}^2 l^3 C^2 e^{-Cl} - 4\,\bar{x}^3 C^2 l^2 e^{-Cl} + 4\,l^4 C \\ & - 16\,\bar{x}l^3 C + 24\,\bar{x}^2 l^2 C + 16\,\bar{x}l^3 Ce^{-1/2\,Cl} + 16\,\bar{x}l^3 Ce^{1/2\,Cl} - 48\,\bar{x}^2 l^2 Ce^{-1/2\,Cl} \\ & - 48\,\bar{x}^2 l^2 Ce^{1/2\,Cl} + 32\,\bar{x}^3 lCe^{-1/2\,Cl} + 32\,\bar{x}^3 lCe^{1/2\,Cl} - 96\,\bar{x}^2 le^{-1/2\,Cl} + 8\,l^3 e^{C\bar{x}} \\ & - 8\,l^3 e^{-C\bar{x}} - 16\,l^3 e^{1/2\,Cl} + 16\,l^3 e^{-1/2\,Cl} - 64\,\bar{x}^3 e^{1/2\,Cl} - 8\,\bar{x}l^3 Ce^{Cl} \\ & - 8\,\bar{x}l^3 Ce^{-Cl} + 36\,\bar{x}^2 l^2 Ce^{Cl} + 36\,\bar{x}^2 l^2 Ce^{-Cl} - 32\,\bar{x}^3 e^{-Cl} + 8\,l^3 e^{Cl} \\ & - 24\,\bar{x}^3 lCe^{-Cl} - 48\,\bar{x}^2 le^{Cl} + 48\,\bar{x}^2 le^{-Cl} + 4\,\bar{x}^3 C^2 l^2 e^{Cl} + 32\,\bar{x}^3 e^{Cl} \\ & - 2\,\bar{x}l^4 C^2 e^{-Cl} - 6\,\bar{x}^2 l^3 C^2 e^{Cl} \end{aligned} \tag{2.30}$$

$$\begin{aligned}\bar{R}_5(\bar{x}) = {} & 24\,e^{1/2\,C(-2\,\bar{x}+l)}l^2 - 24\,e^{-1/2\,C(-2\,\bar{x}+l)}l^2 - 8\,e^{1/2\,C(-2\,\bar{x}+l)}l^3 C + 8\,\bar{x}^3 C^2 le^{-1/2\,Cl} \\ & - 96\,C\bar{x}^2 le^{-1/2\,Cl} + 12\,C\bar{x}^2 le^{Cl} - 8\,\bar{x}^3 C^2 le^{1/2\,Cl} + 12\,C\bar{x}^2 le^{-Cl} - 4\,C^2\bar{x}^2 l^2 e^{Cl} \\ & - 16\,\bar{x}^3 Ce^{Cl} - C^2\bar{x}l^3 e^{-Cl} - 16\,\bar{x}^3 Ce^{-Cl} + e^{C(-\bar{x}+l)}l^3 C + 4\,C^2\bar{x}^2 l^2 e^{-Cl} \\ & - 48\,C\bar{x}l^2 + 168\,C\bar{x}^2 l + 8\,C^2\bar{x}l^3 e^{-1/2\,Cl} + 8\,l^3 Ce^{-1/2\,Cl} - 8\,C^2\bar{x}l^3 e^{1/2\,Cl} \\ & - 4\,\bar{x}^3 C^2 le^{-Cl} - l^3 Ce^{Cl} - 96\,\bar{x}^3 C - 96\,C\bar{x}^2 le^{1/2\,Cl} + e^{-C(-\bar{x}+l)}l^3 C \\ & + 24\,C\bar{x}l^2 e^{1/2\,Cl} + 24\,C\bar{x}l^2 e^{-1/2\,Cl} + 20\,C^2\bar{x}^2 l^2 e^{1/2\,Cl} - 20\,C^2\bar{x}^2 l^2 e^{-1/2\,Cl} \\ & + C^2\bar{x}l^3 e^{Cl} + 4\,\bar{x}^3 C^2 le^{Cl} + 8\,l^3 Ce^{1/2\,Cl} - 8\,e^{-1/2\,C(-2\,\bar{x}+l)}l^3 C + 10\,l^3 C \\ & - l^3 Ce^{-Cl} - 24\,e^{-C\bar{x}}l^2 + 24\,e^{C\bar{x}}l^2 + 24\,l^2 e^{-1/2\,Cl} - 24\,l^2 e^{1/2\,Cl} \\ & + 64\,\bar{x}^3 Ce^{1/2\,Cl} + 64\,\bar{x}^3 Ce^{-1/2\,Cl} - 5\,e^{-C\bar{x}}l^3 C - 5\,e^{C\bar{x}}l^3 C \end{aligned} \tag{2.31}$$

$$\begin{aligned}\bar{R}_6(\bar{x}) = {} & -40\,\bar{x}^3 Cl - 24\,\bar{x}^2 le^{1/2\,Cl} - 32\,\bar{x}^3 e^{-1/2\,Cl} - l^3 e^{-C(-\bar{x}+l)} - 2\,l^4 e^{1/2\,C(-2\,\bar{x}+l)}C \\ & + l^3 e^{C(-\bar{x}+l)} + 4\,\bar{x}^3 lCe^{Cl} + 4\,l^3 e^{1/2\,C(-2\,\bar{x}+l)} - 4\,l^3 e^{-1/2\,C(-2\,\bar{x}+l)} - l^4 e^{-C\bar{x}}C \\ & - l^4 e^{C\bar{x}}C - 2\,l^4 e^{-1/2\,C(-2\,\bar{x}+l)}C + l^3 e^{-Cl} + 2\,l^4 C - 10\,\bar{x}l^3 C + 48\,\bar{x}^2 l^2 C \\ & + 4\,\bar{x}l^3 Ce^{-1/2\,Cl} + 2\,\bar{x}l^4 C^2 e^{-1/2\,Cl} + 4\,\bar{x}l^3 Ce^{1/2\,Cl} - 2\,\bar{x}l^4 C^2 e^{1/2\,Cl} \\ & - 20\,\bar{x}^2 l^2 Ce^{-1/2\,Cl} - 6\,\bar{x}^2 l^3 C^2 e^{-1/2\,Cl} - 20\,\bar{x}^2 l^2 Ce^{1/2\,Cl} + 6\,\bar{x}^2 l^3 C^2 e^{1/2\,Cl} \\ & + 16\,\bar{x}^3 lCe^{-1/2\,Cl} + 4\,\bar{x}^3 C^2 l^2 e^{-1/2\,Cl} + 16\,\bar{x}^3 lCe^{1/2\,Cl} - 4\,\bar{x}^3 l^2 C^2 e^{1/2\,Cl} \\ & + 2\,l^4 Ce^{1/2\,Cl} + 2\,l^4 Ce^{-1/2\,Cl} + 24\,\bar{x}^2 le^{-1/2\,Cl} + 5\,l^3 e^{C\bar{x}} - 5\,l^3 e^{-C\bar{x}} \\ & - 4\,l^3 e^{1/2\,Cl} + 4\,l^3 e^{-1/2\,Cl} + 32\,\bar{x}^3 e^{1/2\,Cl} + \bar{x}l^3 Ce^{Cl} + \bar{x}l^3 Ce^{-Cl} - 4\,\bar{x}^2 l^2 Ce^{Cl} \\ & - 4\,\bar{x}^2 l^2 Ce^{-Cl} + 16\,\bar{x}^3 e^{-Cl} - l^3 e^{Cl} + 4\,\bar{x}^3 lCe^{-Cl} + 12\,\bar{x}^2 le^{Cl} \\ & - 12\,\bar{x}^2 le^{-Cl} - 16\,\bar{x}^3 e^{Cl} \end{aligned} \tag{2.32}$$

$$D(\bar{x}) = -36\,Cl - 48\,e^{-1/2\,Cl} + 24\,e^{-Cl} + 48\,e^{1/2\,Cl} - 24\,e^{Cl} + 8\,lCe^{-1/2\,Cl} + 8\,lCe^{1/2\,Cl} + 10\,lCe^{-Cl} - 4\,l^2C^2e^{1/2\,Cl} + 10\,lCe^{Cl} + 4\,C^2l^2e^{-1/2\,Cl} + C^2l^2e^{-Cl} - C^2l^2e^{Cl} \tag{2.33}$$

The analytical limits of the hybrid basis functions as the rotation speed tends to zero is shown in Eqs. (2.34)–(2.39) which are identical to the shape functions obtained using quintic polynomial.

$$\lim_{C\to 0} N_1 = \frac{-23\,\bar{x}^2l^3 + 24\,\bar{x}^5 - 68\,\bar{x}^4l + 66\,\bar{x}^3l^2 + l^5}{l^5} \tag{2.34}$$

$$\lim_{C\to 0} N_2 = \frac{\bar{x}\left(-12\,\bar{x}^3l - 6\,\bar{x}l^3 + l^4 + 13\,\bar{x}^2l^2 + 4\,\bar{x}^4\right)}{l^4} \tag{2.35}$$

$$\lim_{C\to 0} N_3 = \frac{16\bar{x}^2\left(l^2 + \bar{x}^2 - 2\,l\bar{x}\right)}{l^4} \tag{2.36}$$

$$\lim_{C\to 0} N_4 = \frac{-8\bar{x}^2\left(5\,\bar{x}^2l + l^3 - 4\,\bar{x}l^2 - 2\,\bar{x}^3\right)}{l^4} \tag{2.37}$$

$$\lim_{C\to 0} N_5 = \frac{\bar{x}^2\left(7\,l^3 - 24\,\bar{x}^3 + 52\,\bar{x}^2l - 34\,\bar{x}l^2\right)}{l^5} \tag{2.38}$$

$$\lim_{C\to 0} N_6 = \frac{-8\,\bar{x}^4l - \bar{x}^2l^3 + 5\,\bar{x}^3l^2 + 4\,\bar{x}^5}{l^4} \tag{2.39}$$

Variation of the shape functions corresponding to end degrees of freedom along the element ($N = 1$) is shown in Figs. 2.8 and 2.9 with the conventional Hermite cubic, fifth order and the stiff string basis functions at low and high speeds of $\lambda = 12$ and $\lambda = 100$, respectively. The fifth order polynomial here is based on the 6 degree of freedom element in Fig. 2.1 with three nodes for each element. It is observed that at low rotation speed the present basis functions are similar to the fifth order basis functions as it is observed from analytical limits given in Eqs. (2.34)–(2.39). Also, at low rotation speeds, the stiff-string basis functions are similar to that of the Hermite cubic basis functions, as shown in Ref. [7]. As the rotation speed increases the effect of rotation on shape functions and their deviation from the other basis functions can be clearly observed in Figs. 2.10 and 2.11. At high rotation speeds the stiff string basis function approach linear variation for displacement and become zero for slopes. The new hybrid element captures the slope behavior of the stiff string functions at high rotation speed while retaining the polynomial like displacement behavior for the displacements.

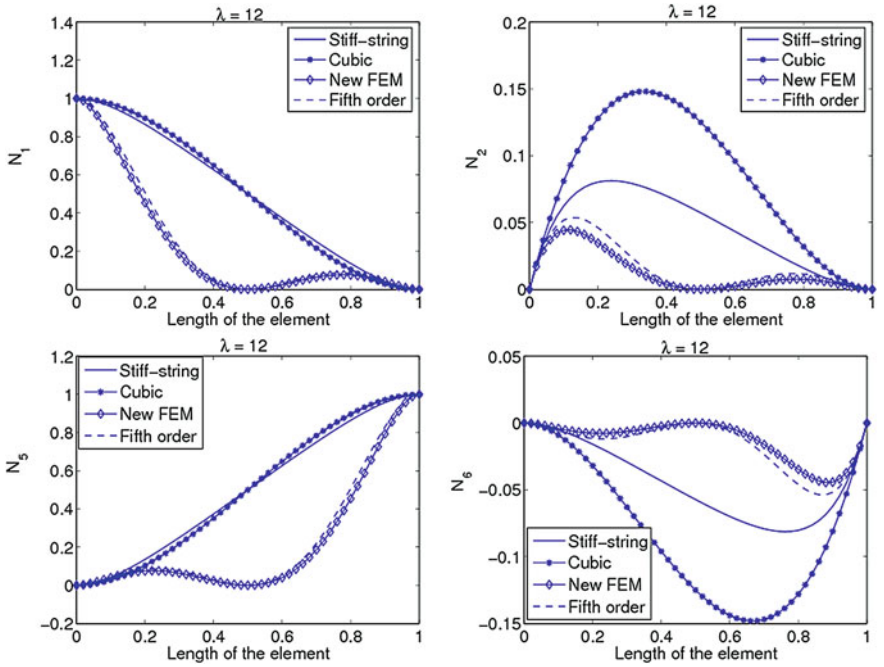

Fig. 2.8 Variation of shape functions ($N = 1, \lambda = 12$) with the new, stiff-string, conventional cubic and fifth order finite elements

2.6 Finite Element

The present improved basis functions are now used to develop the finite element equations for free vibration of the rotating beam. The mass and stiffness matrices can be obtained using the energy expressions. The kinetic energy for a rotating beam is given by

$$T = \frac{1}{2}\int_0^L m(x)\,[\dot{w}(x,\ t)]^2 dx \tag{2.40}$$

where, $\dot{w}(x,\ t)$ is the derivative of $w(x,\ t)$ with respect to time t. The potential/strain energy is given by

$$U = \frac{1}{2}\int_0^L EI(x)\,[w''(x,\ t)]^2 dx + \frac{1}{2}\int_0^L T(x)\,[w'(x,\ t)]^2 dx \tag{2.41}$$

The mass and stiffness matrices ($\mathbf{M}_i$ and $\mathbf{K}_i$) for a beam element can be obtained from the above energy expressions. The calculations for these matrices involve calculating the following integrals:

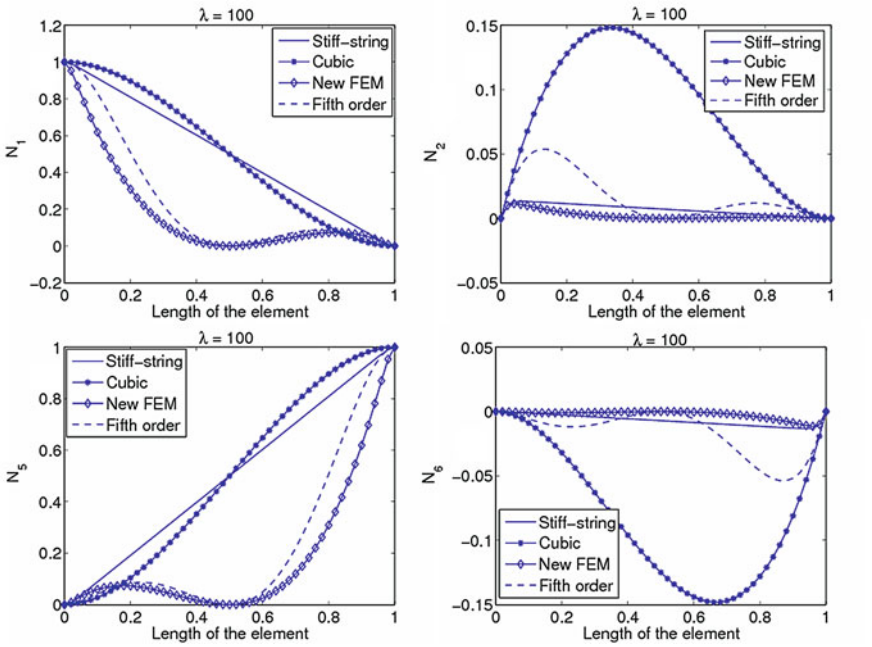

Fig. 2.9 Variation of shape functions ($N = 1$, $\lambda = 100$) with the new, stiff-string, conventional cubic and fifth order finite elements

$$\mathbf{M}_i = \int_0^l m_i(\bar{x})\, \mathbf{N}^T\, \mathbf{N} d\bar{x} \tag{2.42}$$

$$\mathbf{K}_i = \int_0^l EI_i(\bar{x})(\mathbf{N}'')^T\, \mathbf{N}'' d\bar{x} + \int_0^l T_i(\bar{x})(\mathbf{N}')^T\, \mathbf{N}' d\bar{x} \tag{2.43}$$

where

$$T_i(\bar{x}) = \sum_{j=i}^{N} \int_{x_j}^{x_{j+1}} m_j(\bar{x})\Omega^2 \bar{x} d\bar{x} - \int_{x_i}^{x_i+\bar{x}} m_i(\bar{x})\Omega^2 \bar{x} d\bar{x} \tag{2.44}$$

Here $x_i = (i-1)l$ as a uniform mesh is used. Note that no approximations are made regarding the spatial variation in $T(x)$ when deriving the element energy expressions. These assumptions are only made to derive the present hybrid basis functions. The element matrices are then assembled and the boundary conditions applied to get the global stiffness matrix $\mathbf{K}$ and global mass matrix $\mathbf{M}$. The natural frequencies (ω) are then obtained by solving the eigenvalue problem given as

$$\mathbf{K}\Phi = \omega^2\, \mathbf{M}\Phi \tag{2.45}$$

Several numerical examples are now considered and the predictions of the new element are compared with the published literature.

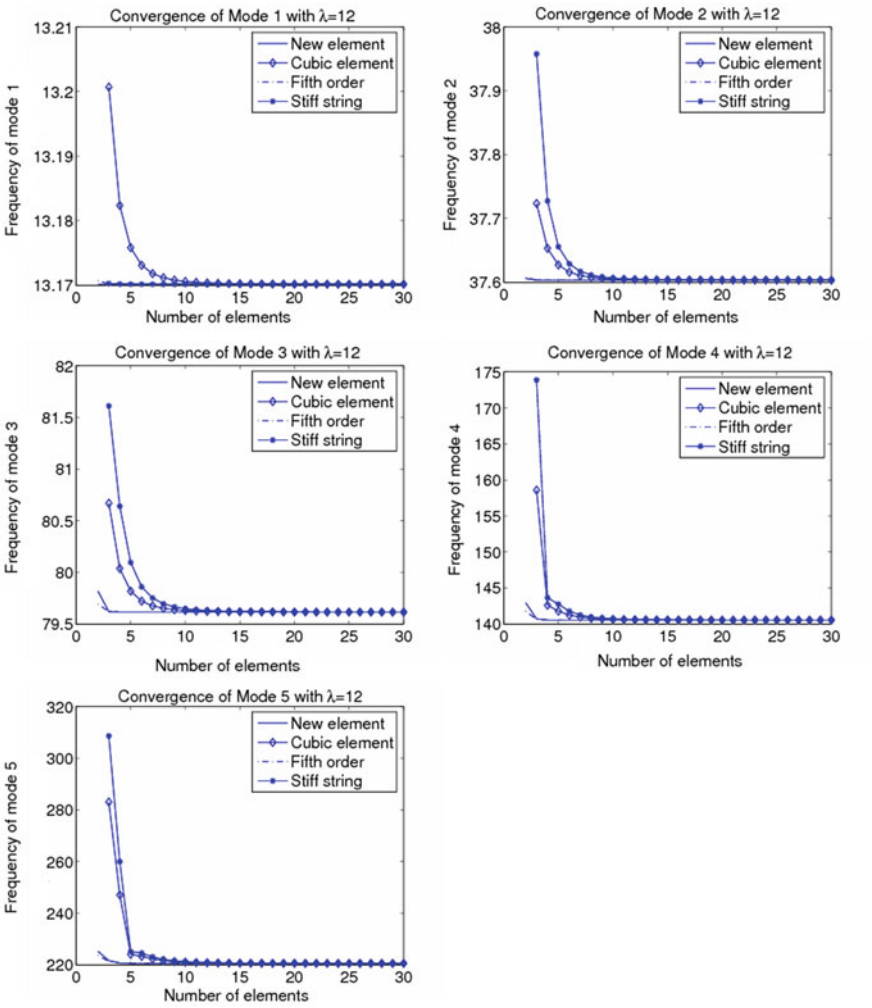

Fig. 2.10 Convergence of the natural frequencies for uniform rotating cantilever beam with $\lambda = 12$

2.6.1 Uniform Rotating Beam

For uniform beams, $m(x)$ and $EI(x)$ are constant throughout the span. Table 2.4 shows a comparison of non-dimensional natural frequencies of a rotating uniform cantilever beam with results from Hodges and Rutkowsky [1], Wright et al. [5] and Wang and Wereley [6]. Convergence for the first five modes was achieved using 10 uniform finite elements in contrast to the stiff-string basis functions [7] which requires 75 uniform finite elements, primarily because of slow convergence of the higher modes.

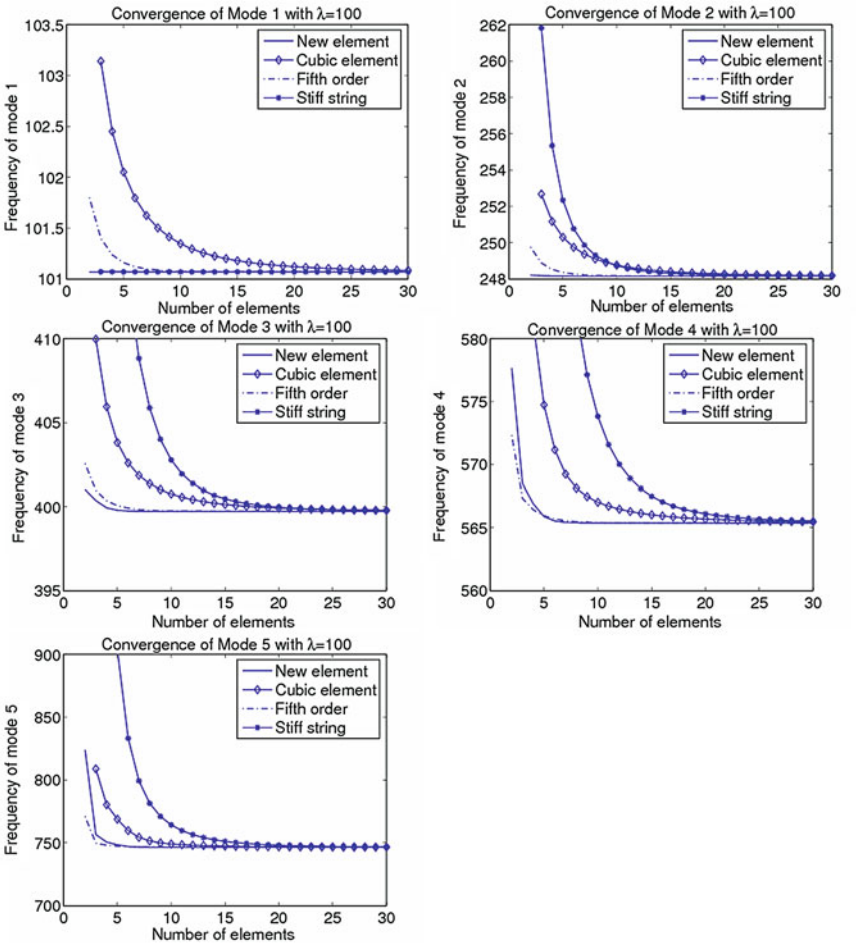

Fig. 2.11 Convergence of the natural frequencies for uniform rotating cantilever beam with $\lambda = 100$

Similar results are obtained for rotating hinged uniform beam and compared with the results from published literature in Table 2.5.

A convergence study is done at two different rotation speeds ($\lambda = 12$ and 100) on the first five modes, since they are commonly used in structural applications. The convergence behaviour of the present basis functions at low and high rotation speeds can be seen in Figs. 2.10 and 2.11 along with the other basis functions. We see that the stiff string basis functions work very well for the fundamental mode. However, their convergence is slow for all the other modes. In contrast, the polynomial work well at the higher modes. It is observed that the convergence of the present basis functions is similar to that of the fifth order basis functions at $\lambda = 12$ as both the shape functions are identical to each other at $\lambda = 12$. As the rotation speed increases, the present basis

Table 2.4 Comparison of non-dimensional natural frequencies of rotating uniform cantilever beam

Mode	Present-FEM	Wang and Wereley [6]	Wright et al. [5]	Hodges et al. [1]
$\lambda = 12$				
1	13.1702	13.1702	13.1702	13.1702
2	37.6031	37.6031	37.6031	37.6031
3	79.6145	79.6145	79.6145	79.6145
4	140.534	140.534	140.534	N/A
5	220.537	220.536	220.536	N/A

Table 2.5 Comparison of non-dimensional natural frequencies of rotating uniform hinged beam

Mode	Present-FEM	Wang and Wereley [6]	Wright et al. [5]
$\lambda = 12$			
1	12.0000	12.0000	12.0000
2	33.7603	33.7603	33.7603
3	70.8373	70.8373	70.8373
4	126.431	126.431	126.431
5	201.123	201.122	201.122

bunctions are better able to capture the rotation effects and significant improvement in convergence for the higher modes can be clearly seen from the Fig. 2.11. Especially, the convergence of the first three modes is significantly improved at high rotation speeds.

An important point to note is that the present FEM needs only one element for the first mode to converge to an accuracy of less than 0.0001 at any high rotation speed. The present FEM also requires only 10 uniform finite elements for the convergence of first five modes to the accuracy of 0.0001 at $\lambda = 12$. Thus the element is effective at both low and high speeds.

Table 2.6 shows the number of elements required to converge the first five frequencies to an accuracy of less than four decimal places with various basis functions considered at a rotation speed of $\lambda = 100$. It is evident that the hybrid basis functions requires fewer number of elements to converge to the desired accuracy as compared to the other basis functions which can require a very high number of elements. It should however be mentioned that the stiff string and cubic elements have one node lesser than the new element and fifth order element. The total number of degrees of freedom for these cases is therefore also given in Table 2.7. It is to be noted that the degrees of freedom required by the new element are much less compared to that for cubic and stiff string cases, and also quite less compared to the fifth order polynomial.

The mode shapes corresponding to $\lambda = 12$ and 100 are shown in Fig. 2.12. At high rotation speeds, the fundamental mode becomes linear as the centrifugal stiffening effect overwhelms the flexural stiffness effect for the mode.

Table 2.6 Comparison of number of elements required with various basis functions to get the converged frequency to the accuracy of < 0.0001 for rotating uniform cantilevered beam ($\lambda = 100$)

Mode no.	New element	Fifth order	Stiff string	Cubic
1	1	20	4	129
2	8	23	128	187
3	11	26	163	183
4	14	28	203	198
5	17	31	333	286

Table 2.7 Comparison of degrees of freedom with various basis functions to get the converged frequency to the accuracy of < 0.0001 for rotating uniform cantilevered beam ($\lambda = 100$)

Mode no.	New element	Fifth order	Stiff string	Cubic
1	4	80	8	258
2	32	92	256	374
3	44	104	326	366
4	56	112	406	396
5	68	124	666	572

2.7 Tapered Rotating Beam

In order to validate the robustness of the new finite element with the hybrid basis functions, two different types of linearly tapered beams are chosen from the published literature. These beams and the results are given by Hodges and Rutkowsky [1] and Wright et al. [5].

In general, we assume that variation of mass along the beam length is defined as

$$m(\xi) = m_0 \, (1 - \alpha \, \xi) \tag{2.46}$$

where m_0 correspond to value of mass per unit length at the thick end of the beam ($\xi = 0$), α is the taper parameter such that $0 < \alpha < 1$. Note that $\alpha \neq 1$, which results in singularity at $\xi = 1$. Flexural stiffness variation along the length of beam element is defined as

$$EI(\xi) = EI_0 \, (1 - \beta_1 \, \xi - \beta_2 \, \xi^2 - \beta_3 \, \xi^3 - \beta_4 \, \xi^4) \tag{2.47}$$

where EI_0 corresponds to the value of flexural rigidity at the thick end of the beam ($\xi = 0$). Here $\beta_i, i = 1, 4$, are taper parameters for the stiffness distribution. These parameters can be determined by using α for beams with a rectangular cross-sectional

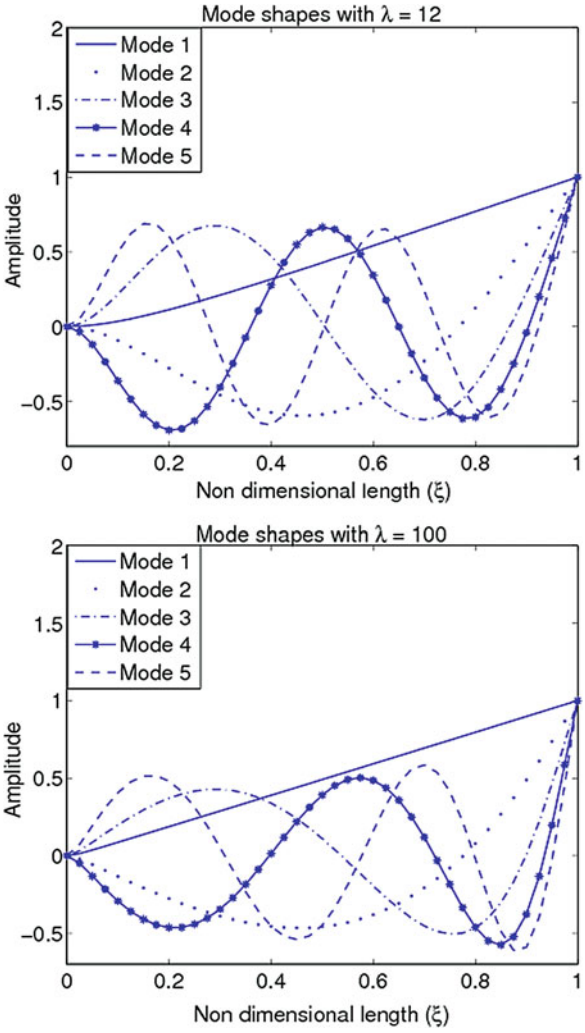

Fig. 2.12 Mode shapes of uniform rotating cantilever beam with $\lambda = 12$ and 100

area and thickness varying along the beam length. However, as with the example studied by Wright et al. [5], the taper parameters for mass and flexural stiffness are not necessarily related. They are independent variables. However, these parameters should not result in a singularity for flexural stiffness at $\xi = 1$. Two numerical examples based on special cases of Eqs. (3.40) and (3.41) are considered next (Table 2.8).

Table 2.8 Comparison of non-dimensional natural frequencies of hinged tapered beam linear (Example 1)

Mode	Present-FEM	Wang and Wereley [6]	Wright et al. [5]
$\lambda = 12$			
1	12.0000	12.0000	12.0000
2	30.7745	30.7741	30.7745
3	63.1722	63.1758	63.1722
4	112.090	112.040	112.090
5	178.016	178.978	178.105

Table 2.9 Comparison of non-dimensional natural frequencies of cantilever tapered beam (Example 2)

Mode	Present-FEM	Wang and Wereley [6]	Wright et al. [5]
$\lambda = 12$			
1	14.0313	14.0313	14.0313
2	35.9064	35.9060	35.9064
3	72.8565	72.8604	72.8565
4	126.401	126.336	126.401
5	198.880	198.243	198.880

Example 1 (Linear Mass, Linear Stiffness, Cantilevered Beam)

In the first example, the tapered beam used by Wright et al. [5] is considered. For this particular problem, the taper is such that the mass per unit length is $m(\xi) = m_0\,(1 - 0.8\,\xi)$ and the bending flexural rigidity is $EI(\xi) = EI_0\,(1 - 0.95\,\xi)$.

The results obtained for this case are compared with those of Wright et al. [5] and Wang and Wereley [6]. Table 2.9 shows the comparison of our results with their works for the first five modes at $\lambda = 12$. Our results compare very well with the published results using only 10 tapered finite elements. Wang and Wereley [6] used a single spectral finite element which requires 350 terms in the Frobenius power series solution. Wright et al. [5] method is also based on a similar principle of using a power series as that of Wang and Wereley [6].

Convergence Study for Tapered Rotating Beam (Example 1)

The convergence behaviour for the tapered rotating beam considered in this example can be clearly seen from the Figs. 2.13 and 2.14. Again the significant improvement in convergence using the new shape functions is clearly evident. The hybrid shape functions work well both at high and low rotation speeds. For the fundamental mode, the new shape functions act like stiff string polynomials, and are also able to act like polynomials for the higher modes.

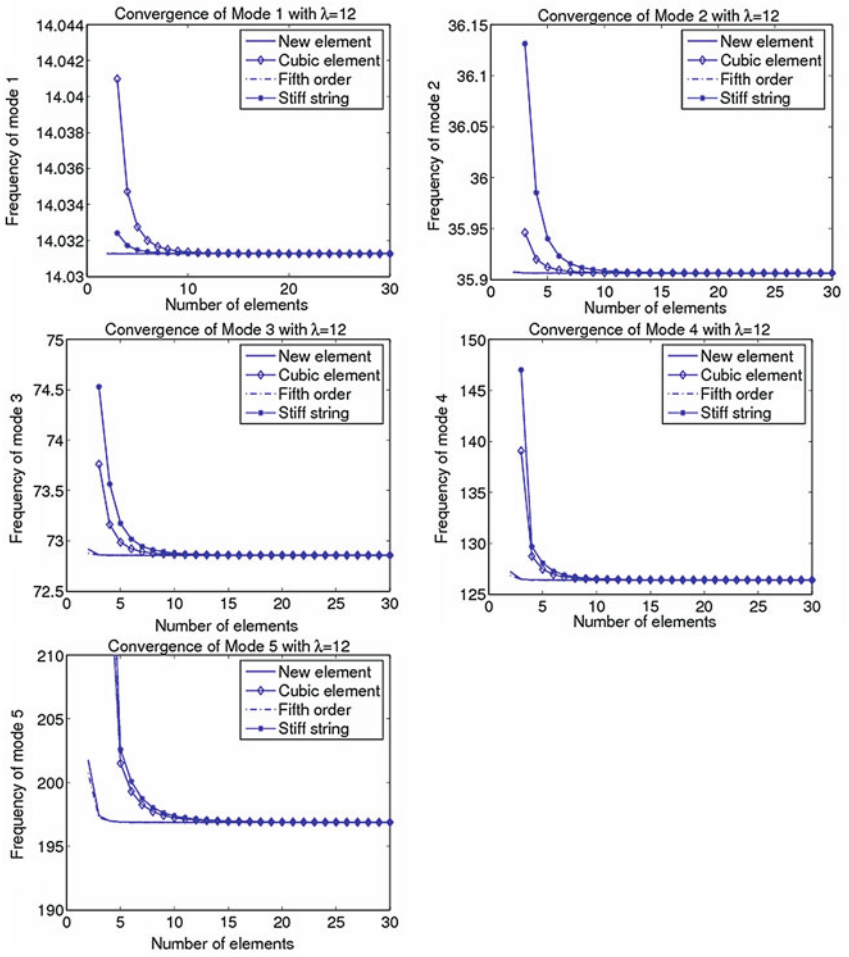

Fig. 2.13 Convergence of the natural frequencies for tapered rotating cantilever beam with $\lambda = 12$

Example 2 (Linear Mass, Linear Stiffness, Hinged Beam)

In the third example, the tapered beam used by Wright et al. [6] with hinged boundary conditions is considered. For this particular problem, the taper is such that both the mass per unit length is $m(\xi) = m_0\,(1 - 0.8\,\xi)$, and the bending flexural rigidity is $EI(\xi) = EI_0\,(1 - 0.95\,\xi)$. The results obtained using the present FEM for first five modes are compared with those of published literature in Table 2.10. It can therefore be concluded that the present FEM works well for beams with various mass and stiffness tapers.

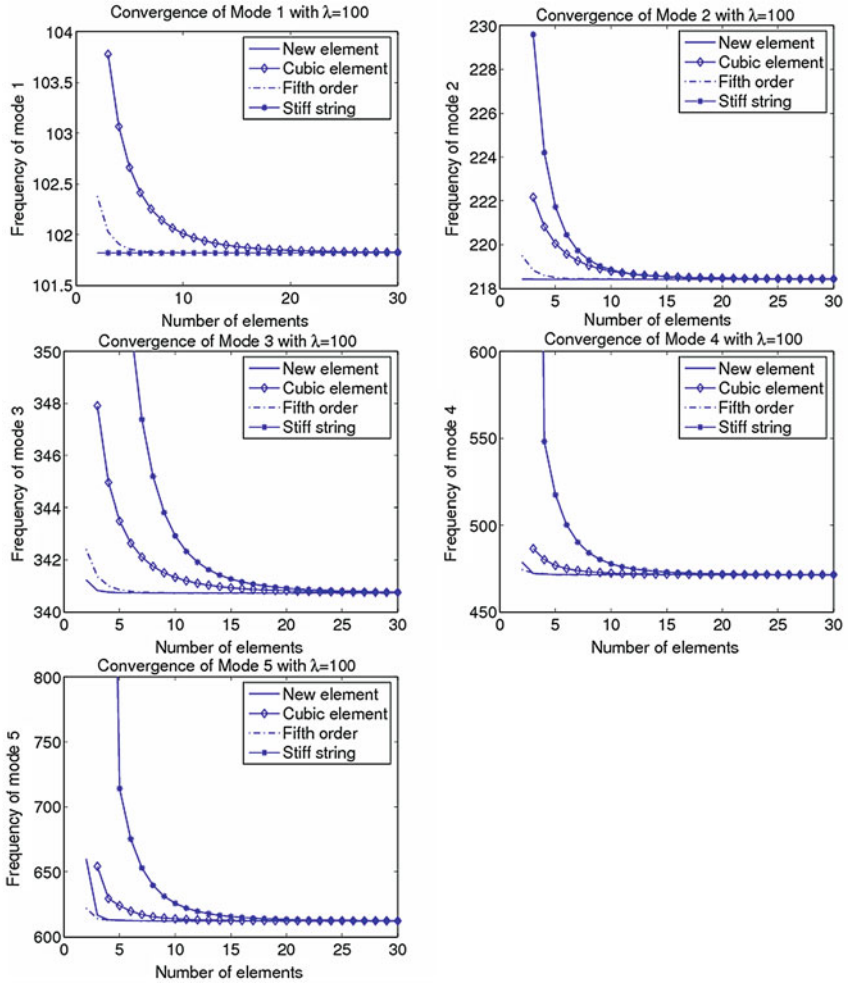

Fig. 2.14 Convergence of the natural frequencies for tapered rotating cantilever beam with $\lambda = 100$

Example 3 (Linear Mass, Cubic Stiffness, Cantilevered Beam)

In this example, the taper is such that the variation of the mass per unit length is $m(\xi) = m_0\,(1 - 0.5\,\xi)$, and the bending flexural rigidity is $EI(\xi) = EI_0\,(1 - 0.5\,\xi)^3$. This type of tapered beam is used by Hodges and Rutkowsky [1] for analysis. These equations cover all the beams of a solid rectangular cross section with a constant width and linearly varying depth. The results obtained for this case are compared with those obtained by Wang and Wereley [6], and Hodges and Rutkowsky [1] in Table 2.11. Results for higher modes are not available in the published literature. Therefore, the comparison of only three modes is shown in this table. It can be observed that the comparison is very good.

Table 2.10 Comparison of non-dimensional natural frequencies of hinged tapered beam (Example 2)

Mode	Present-FEM	Wang and Wereley [6]	Wright et al. [5]
$\lambda = 12$			
1	12.0000	12.0000	12.0000
2	30.7745	30.7741	30.7745
3	63.1722	63.1758	63.1722
4	112.090	112.040	112.090
5	178.016	178.978	178.105

Table 2.11 Comparison of non-dimensional natural frequencies of cantilever tapered beam (Example 3)

Mode	Present-FEM	Ref. [6]	Ref. [1]
$\lambda = 12$			
1	13.4711	13.4711	13.4711
2	34.0877	34.0877	34.0877
3	65.5237	65.5237	65.5237

2.8 Summary

In the present chapter, new shape functions are derived for rotating beams, by using the exact solution of the homogenous part of the governing static differential equation of a stiff string. In this case, the shape functions are not only functions of the element length, but also they are functions of rotation speed, element location across the beam, element mass and stiffness, mass of outboard elements, and length of the beam. The element shows superior convergence of the first two modes at high rotation speed over the conventional Hermite cubics and also presents a new shape function for rotating beams which capture the effect of centrifugal force and element location. The poor convergence of the fundamental mode at high rotation speeds using the cubic polynomials is solved by using the stiff string basis functions. This new element is also applied to determine the natural frequencies of uniform and tapered rotating beams and the results compare very well with the published results.

In the present chapter, hybrid basis functions are also derived for rotating beams by using the linear combination of terms from the exact solution of static homogenous differential equation of a stiff string and that of a non-rotating beam. The shape functions are not only functions of the element length, but also they are functions of rotation speed, element location across the beam, element mass and stiffness, mass of outboard elements, and length of the beam. The new element shows superior convergence for the first five modes considered compared to the stiff-string, conventional fifth order and Hermite cubic based finite elements and also presents a new shape function for rotating beams which capture the effect of centrifugal force and

element location. The new element alleviates the convergence difficulties posed by the stiff-string functions in predicting the frequencies corresponding to higher modes at high rotation speeds. It also overcomes the difficulty which the polynomials have in predicting the fundamental mode at high rotation speeds. The robustness of the proposed element is demonstrated by determining the natural frequencies of the uniform and tapered rotating beams and the corresponding results shows an excellent corelation with the published results.

References

1. Hodges DJ, Rutkowsky MJ (1981) Free vibration analysis of rotating beams by a variable order finite element method. AIAA J 19(11):1459–1466
2. Pesheck E, Pierre C, Shaw SW (2002) Modal reduction of a nonlinear rotating beam through nonlinear normal modes. ASME J Vib Acoust 124(2):229–236
3. Chakraborty A, Gopalakrishnan S, Reddy JN (2003) A new beam finite element for the analysis of functionally graded materials. Int J Mech Sci 45(3):519–539
4. Fletcher H (1964) Normal vibration frequencies of a stiff string. J Acoust Soc Am 36(1):203–210
5. Wright AD, Smith CE, Thresher RW, Wang JLC (1982) Vibration modes of centrifugally stiffened beams. J Appl Mech 49(2):197–202
6. Wang G, Wereley NM (2004) Free vibration analysis of rotating blades with uniform tapers. AIAA J 42(12):2429–2437
7. Gunda JB, Ganguli R (2008) Stiff-string basis functions for vibration analysis of high speed rotating beams. J Appl Mech 75(2):0245021–0245025
8. Bathe KJ (1996) Finite element procedures. Prentice Hall, Upper Saddle River

http://www.springer.com/978-981-10-1901-2

Finite Element Analysis of Rotating Beams
Physics Based Interpolation
Ganguli, R.
2017, XII, 283 p. 108 illus., 19 illus. in color., Hardcover
ISBN: 978-981-10-1901-2